RAY TRACING RADIO WAVES IN WILDFIRE ENVIRONMENTS

K. Mphale

Physics Department
University of Botswana
P/Bag 0022. Gaborone, Botswana

M. Heron

Marine Geophysical Laboratory
James Cook University
Townsville Q4811, Australia

Abstract—Wildfires are uncontrolled exothermic oxidation of vegetation. Flame combustion temperatures could be in excess of 1600 K. Under the high temperature environment, plants' organic structure crumbles to release omnipresent alkali nutrients into the combustion zone. The alkali based compounds thermally decomposed to constituent atoms which ultimately ionised to give ions and electrons. The presence of electrons in the flame lowers its refractive index, thereby creating a medium of spatially varying refractive index. In the medium, incident radio waves change speed and are consequently deflected from their original path. The refraction has an effect of decreasing signal intensity at a targeted receiver which is at the same height as a collimated beam transmitter which is at a considerable distance away from the former. A numerical experiment was set to investigate the sub refractive behaviour of a very high intensity eucalyptus wildfire $(90 \, \mathrm{MWm}^{-1})$ plume using two dimensional (2D) ray tracing scheme. The scheme traces radio rays as they traverse the plume. The ratio of number rays in a collimated beam reaching the targeted receiver to number of rays leaving the transmitter is used to calculate signal intensity loss in decibels (dB) at the receiver. Assuming an average natural plant alkali (potassium) content of 0.5%, attenuation (dB) was observed to be factor of both propagation frequency and temperature at the seat of the fire plume; and only of temperature at cooler parts of

the plume. The 2D ray tracing scheme predicted a maximum attenuations of 14.84 and 5.47 dB for 3000 and 150 MHz respectively at 0.8 m above canopy-flame interface over propagation path of 48.25 m. An attenuation of 0.85 dB was predicted for frequencies from 150–3000 MHz over the same propagation distance at plume height of 52.8 m above ground.

1. INTRODUCTION

Southwest Western Australia experiences a Mediterranean climate, thus predominate dry summers and cool wet winters. Conditions exist in summer when the region experiences strong dry windy conditions and at times, heat waves. The influx of hot dry air in to the region causes dehydration and heat stress conditions in the endodermic eucalyptus species. This ultimately leads to very high intensity wildfires (>7000 kWm^{-1}) when the dry storms concur with the adverse atmospheric conditions.

About 3.4% of plant's dry mass is the element potassium [6]. The element exist ionically or organically attached to oxygen-containing functional groups (i.e., O-C-) of the organic structure of plants, as discrete particles in voids of the organic matrix and in solution form such as in xylem vessels. During a wildfire, the metal species are released from a thermally crumbling plant structure and convectively drawn into the combustion zone of the fire. Potassium species are a large fraction of inorganic emissions during vegetation combustion [13].

Wildfire combustion zone is characterized by high enough temperatures to cause thermal dissociation of potassium species. Potassium species have low dissociation energies (e.g., 3.79 eV for K_2CO_3). From studies of nutrient cycling, up to 28% of inherent potassium in plants is volatilized at combustion efficiency of 98% [7]. Vodacek et al. [15] also estimate that 10–20% of potassium in vegetation is ionized in wildfires. This makes wildfires a weakly ionized environment that affects troposheric radio refractivity.

During a wildfire suppression, Australian fire brigades use two-way Very High and Ultra High Frequency (VHF/UHF) mobile radio sets for communication. The mobile radio sets have omnidirectional antennas. Despite having omnidirectional antennas, there are anecdotal reports of failure for the two-way mobile radio systems to maintain Line-Of-Sight (LOS) communication on fire grounds e.g., in Williams et al. [16] and Foster, [17]. This is a safety concern for fire fighters as efficient radio communication is desirable at all times during suppression. It is therefore important to establish scientific basis for the anecdotal

reports. The paper investigates radio wave refraction in wildfire environments. Refraction is one of the possible ways that could affect LOS radio wave communication in high intensity fire environments where significant radio refractive index gradients exist.

2. IONISATION IN WILDFIRES

2.1. Thermal Ionisation

Wildfires are an exothermic oxidation reaction in nature, fierce temperatures in the range up to 2000°C [14] are produced in its reaction zone. The very hot environment thermally excites flame particles, and the particles are consequently thermally ionised to produce electrons and ions on selective basis determined by temperature and ionisation potential. Thermal ionisation of flame species ($S(g)$) occurs by the following process:

$$S(g) \Leftrightarrow S^+(g) + e^-$$ (1)

Species that could appreciably undergo thermal ionisation in a wildfire environment are alkali and alkaline earth metals (e.g., K, Na and Ca) and graphitic carbon (C_n). In essence a wildfire could be considered an impure hydrocarbon diffusion flame seeded with alkalis and alkaline earth metals.

Most of the carbon atoms that exit in wildfire flames are in a coagulated form called soot. Soot is sub-microscopic in size and has graphite structure (infinite large aggregate of carbon atoms) although smaller than the latter. The electrochemical characteristics of soot are different from both carbon and graphite. Ionisation potential (ϕ_{ip}) increases from graphite ($\phi_w = 4.35\,\text{eV}$) to carbon ($\phi_{ip} = 11.26\,\text{eV}$), thus ϕ_{ip} decreases from a small to large carbon structure. Structurally, soot lies between carbon and graphite polymer, therefore it is reasonable to suggest that its ϕ_w should be between 4.35 and 11.26 eV. ϕ_w for soot has been experimentally determined to be 8.5 eV [9]. With ϕ_w almost twice that of potassium, the presence of potassium in flames is then the most effective source of thermal ionisation in wildfires.

Assuming local thermal equilibrium conditions, the ionisation equilibrium constant (K_I) is given by the relation:

$$K_I = 2 \left(\frac{2\pi m_e kT}{h^2}\right)^{3/2} \exp\left(\frac{-(E_i)}{kT}\right)$$ (2)

where k, T, E_i and m_e are Boltzmann's constant, absolute temperature and mass of electron respectively. Electron density (N_e) due to thermal

ionisation of K atoms is related the ionisation equilibrium constant and the total number of ionised K particles (N_p) in the flames as [3]:

$$N_e = (K_1 N_p)^{1/2} \left[\left(1 + \frac{K_1}{4N_p}\right)^{1/2} - \left(\frac{K_1}{4N_p}\right)^{1/2} \right] \tag{3}$$

The total number of ionised K particles (N_p) is related to the potassium atoms in the flame by the equation [3]:

$$N_p = \frac{7.335 \cdot 10^{21} \eta}{T} \text{ cm}^{-3} \tag{4}$$

where η is the number density of K atoms in a wildfire.

2.2. Chemi-ionisation

Chemi-ionisation is another possible mechanism by which significant ionisation may occur in wildfire [4]. In the process, dissociation reactions provide part of the energy required for ionisation since there are exothermic and the rest is from the flame. Exited methyl radical CH^* is a known contributor to ionisation in the hydrocarbon flames e.g., in Sorokin et al. [10]. CH radical reacts with oxygen atoms in the flame to produce CHO^+, a primary ion in hydrocarbon flames and electrons according to the following reaction equation:

$$CH^* + O \Leftrightarrow CHO^+ + e^- \tag{5}$$

The chemi-ionisation reaction mentioned above, temperature and concentration of species hinder their contribution to ionisation. For example, oxygen (O_2) has high dissociation energy $(5.5\,\text{eV})$, therefore the availability of O atoms in equation (5) is temperature and species concentration dependent.

3. WILDFIRE PLUME MODEL

3.1. Structure of a Forest Fire Plume

A wildfire plume is composed of three regions which differ in chemical and physical properties. The differences are mainly on spatial variation of thermo-physical properties e.g., temperature, plume particle velocity and ionization. The regions are the: continuous and intermittent flames; and smoke column and are shown in Fig. 1. The continuous flame is the lower part of the plume close to the vegetation stratum where maximum plume temperature occurs. Intermittent flame region
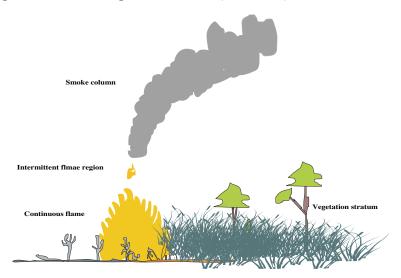
Figure 1. Plume regions in a savanna wildfire.

lies just above the continuous flame region. Balls of flame are observed to come away from the source in the region. Rapid cooling of the plume occurs in the smoke column region. The cooling is attributed to the mixing of emission with entrained ambient air.

3.1.1. Plume Centerline Temperature Variation with Height

Temperature in the centerline of a wildfire plume decays exponentially with height. The temperature decrease with height is given by Weber et al. [12] as:

$$T_{plume} = T_\infty + K \exp\left\{-\beta(z - z_d)^2\right\} \tag{6}$$

where K, Z_d, Z_p are empirical constant, constant related to fuel height, constant related to flame height respectively and $\beta = 1/(2z_p(z_p - z_d))$.

4. WILDFIRE PLUME REFRACTIVE INDEX

4.1. Radio Refractive Index for a Wildfire Plume

Radio refractive index (μ_{fg}) for a gaseous medium is generally given by the relation [18]:

$$\mu_{fg} - 1 = \left(\sum_r K_r n_r\right) \times 10^{-6} \tag{7}$$

where μ_{fg}, K_r and n_r are refractive index, specific refractivity and number concentration of medium constituents respectively.

4.1.1. Flame Refractive Index Due to Unionized Species

Dielectric permittivity (ε) of unionized flame constituent is related to its molecular weight (M) and density (ρ) by the equation [2]:

$$\frac{\varepsilon - 1}{\varepsilon + 2} = \frac{4N_a\pi\rho}{3M}\left[\alpha_0 + \frac{\mu^2}{3kT}\left(\frac{1}{1 + i\omega\tau}\right)\right] \tag{8}$$

where $\omega, \alpha_0, \mu, k, N_a, T$, and τ are electric field frequency, polarization factor for a plume gas, electric moment dipole of the plume gas, Boltzmann's constant, Avogadro's constant, smoke temperature and relaxation time of the molecules to return to their random distribution after an impressed electric field is removed respectively.

At frequencies less than $100\,\mathrm{GHz}$, $\omega\tau \ll 1$ [2] and for most gases, $\varepsilon + 2 \cong 3$, assuming that the gases behave ideally, equation (8) can be approximated to:

$$\varepsilon - 1 = \frac{4N_a\pi P}{RT}\left[\alpha_0 + \frac{\mu^2}{3kT}\right] \tag{9}$$

A compact form of (9) will be

$$\varepsilon - 1 = \frac{k_{fg}P}{T} \tag{10}$$

where k_{fg} is constant for the smoke gases.

As the flame is composed of many gases, the constant k_{fg} can be broken down to account for each flame constituent, each having its own constant. Equation (10) can therefore be written as

$$\varepsilon - 1 = \sum_1^r \frac{k_{fgr}P_{fgr}}{T} \tag{11}$$

where k_{sgr} and P_{sgr} are constant for air or plume gas constituent and its partial pressure.

Permittivity (ε) is related to refractive index (μ_{fg}) by the relation; $\varepsilon - 1 = \mu_{fg}^2 - 1$. Using binomial expansion, $\varepsilon - 1 \approx 2(\mu_{fg} - 1)$.

Therefore (7) for plume gases becomes,

$$\mu_{fg} - 1 = \frac{2N_a\pi \cdot P}{RT}\sum_1^r\left[\alpha_{0r} + \frac{\mu_r^2}{3kT}\right] \tag{12}$$

4.1.2. Refractive Index Due to Unbounded Electrons

Refractive index due to ionization in the flame is related to the radio wave phase shift and attenuation coefficient by the equation [1];

$$\mu_{fg} = \frac{c}{\omega}\beta_f - i\frac{c}{\omega}\alpha_f \tag{13}$$

where $c, \omega, \beta_f, \alpha_f$ are speed of light, phase and attenuation coefficient of an electromagnetic wave in the flame. Phase shift and attenuation induced by weakly ionized gas such as a wildfire is expressed by Akhtar et al. [1] as:

$$\beta_f = \frac{\omega}{c}\left\{\frac{1}{2}(1-s) + \frac{1}{2}\left[(1-s)^2 + (sq)^2\right]^{1/2}\right\}^{1/2} \tag{14}$$

and

$$\alpha_f = \frac{\omega}{c}\left\{-\frac{1}{2}(1-s) + \frac{1}{2}\left[(1-s)^2 + (sq)^2\right]^{1/2}\right\}^{1/2} \tag{15}$$

where $s = \frac{\omega_p^2}{\omega^2 + \varphi_{\text{eff}}^2}$ and $q = \frac{\varphi_{\text{eff}}}{\omega}$. At radio wave frequencies and considering that the wildfire flame is weakly ionized with electron densities up to $10^{16}\,\text{m}^{-3}$ and highly collisional (collision frequency in the range of $10^{11} - 10^{12}\,\text{s}^{-1}$), $Q_{\text{eff}} \gg \omega > \omega_p$. $(1-s)^2 \gg (sq)^2$ in equations (14) and (15), therefore the respectively equations reduce to $\beta_f = \frac{\omega}{c}(1 - \frac{A^2}{2s^2})$ and $\alpha_f = \frac{\omega}{c}(-\frac{A^2}{2s})$, where A is the normalized plasma frequency, ω_p/ω. Complex refractive index (13) can then be written as:

$$\mu_{fg} = \left(1 - \frac{A^2}{2s^2}\right) - i\left(\frac{A^2}{2s}\right) \tag{16}$$

Radio refractivity (N_{fg}) of the wildfire flame is compounded $(\mu_{fg} - 1)$ terms for both the electrons and unionized flame constituents, thus;

$$N_{fg} = \left\{\left[\frac{2 \cdot \pi \cdot P_a}{RT} \cdot \sum_1^r \left[\alpha_{0r} + \frac{\mu_r^2}{3kT}\right] - \frac{1}{2}\left(\frac{A^2}{s^2}\right)\right] - i\left[\frac{A^2}{2s}\right]\right\} \cdot 10^6 \tag{17}$$

5. TWO DIMENSIONAL RAY TRACING SCHEME

5.1. Description of the Scheme

A number of ray tracing schemes have been developed, e.g., in Marchand, [19] and Streifer et al. [11]. The procedures were

mathematically rigorous and relied on analytical refractive index profiles. Ling et al. [5] developed a method based on Fermats principle which did not relying on analytical refractive index profiles. A much simpler ray tracing procedure was later developed by Richerzhagen [8]. The method combined finite element and ray tracing techniques. Though the method could be used for an arbitrary refractive index profile, it had a disadvantage of assuming planar stratification. A ray tracing method that does not assume any stratification is used in the numerical. It is used in the numerical experiment because it is not mathematically rigorous. The ray tracing scheme uses refractive index gradient in to determine direction of ray trajectory. This is much simpler than solving ordinary differential equation to determine ray direction as in [11] and [19]. The scheme has been validated against Ling et al. [5] dielectric space (Eq. (21)) and many others. The scheme was observed to reproduce ray deflections obtained by [5] (see Figure 4). The limitation of the ray tracing scheme is that it is in two dimensions (2D) therefore fails to capture deflections in the third dimension for attenuation calculation. Step-size may also limit the scheme in a media with rapidly varying refractive index.

The scheme traces a radio ray in small steps (segments) through a medium of inhomogeneous refractive index until it emerges from the medium. Initially a ray is projected horizontally or at any direction with respect to the horizontal into the medium. A unit vector of the ray segment (r_u) is then determined as it propagates through the medium. The head of the ray segment marks the point where the refractive index of a medium in which the next ray segment will be traveling is to be determined. The refractive index of the starting ray segment is assumed known (n_0). Figure 2 shows the ray tracing procedure in a non homogeneous refractive medium. At the end of the ray segment a vector normal to a surface of constant refractive index at that point is calculated. The normal at the end of the ray segment is a gradient in refractive index at the point. In two dimensions (2D), a gradient of refractive index is calculated from the relation:

$$\nabla n = \vec{i} \, \frac{\partial n}{\partial x} + \vec{j} \, \frac{\partial n}{\partial y} \tag{18}$$

where $\frac{\partial n}{\partial x}$ and $\frac{\partial n}{\partial y}$ are x and y derivatives. The derivatives are calculated from the following expression, e.g., in x-direction;

$$\frac{\partial n(x,y)}{\partial x} = \frac{n((x+\Delta s),y) - n((x-\Delta s),y)}{2\Delta s} \tag{19}$$

where Δs is a very small step or offset point either side of a ray head. The y derivate can be calculated in a similar way as in equation (19).

Angle of incidence (Φi) = α+β
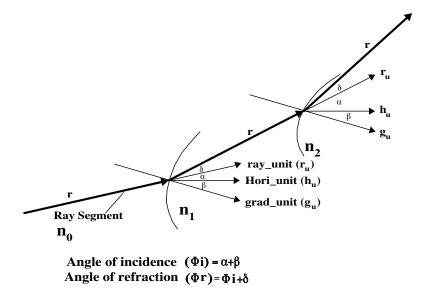**Angle of refraction (Φr) = Φi+δ**

Figure 2. Ray trace through a non-homogeneous plume.

Angles of incidence are determined from the dot product of r_u and gradient unit vector (g_u). From Figure 2, angle of incidence (Φ_i) is the sum of α and β. Angle of refraction (Φ_r) is calculated from Snell's law:

$$\Phi_r = \arcsin\left[\frac{n_{\rho-1}}{n_\rho}\sin(\Phi_i)\right] \tag{20}$$

where $n_{\rho-1}$ and n_ρ are the refractive indices in the trajectory of the previous and present segments. Angle of refraction is also the sum of α, β and δ. The increment in the horizontal and vertical direction are given by $r \cdot \cos(\alpha + \delta)$ and $r \cdot \sin(\alpha + \delta)$ respectively.

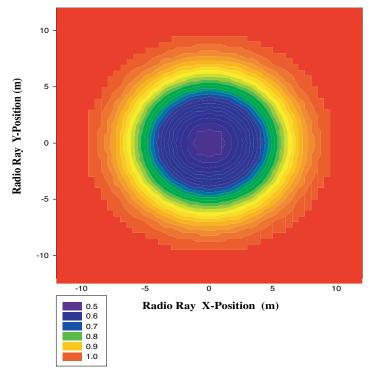## 5.2. Validation of the Ray Tracing Scheme

A dielectric "pothole" with rapidly varying refractive index with radial symmetry was used to validate the 2D ray-tracing scheme. The pothole's refractive index $(n(\rho))$ varies as:

$$n(\rho) = \begin{cases} \sqrt{0.75\left[1 - \frac{1}{3}\cos\left(\frac{\pi\rho}{10}\right)\right]}, & \rho < 10 \\ 1, & \rho > 10 \end{cases} \tag{21}$$

where ρ is the radial distance from the center of the pothole calculated from the x and y coordinate points and is given by;

$$\rho = \sqrt{x^2 + y^2} \tag{22}$$

The permittivity at the center of the pothole is $\sqrt{\frac{1}{2}}$ and is shown below in Fig. 3.

Dielectric pothole for validating a 2D-Ray Tracer

Figure 3. Dielectric pothole used in the validation of the 2D ray tracing scheme.

A similar structure was used by Ling et al. [5] to validate their ray-tracing scheme. From the validation, rays that pass through the center $(0, 0)$ and edge $(0, 10)$ are not refracted, as expected. Figs. 4 and 5 show the validation results. Deviations are decrease just about the center to edges (i.e., Y-position $\cong 0$ to Y-Position $= 10$). The results are very similar to those of Ling et al. [5].
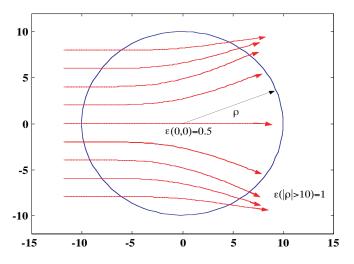
Figure 4. Rays (excluding rays at edges) refraction in a dielectric pothole.

6. NUMERICAL EXPERIMENT

6.1. Eucalyptus Crown Fire

6.1.1. Crown Fire Behavior

The numerical experiment focuses on a very high intensity wildfire which is a common occurrence in Mediterranean regions of Spain and southwestern Australia's dry sclerophyll forests during summer. A wildfire of intensity $16\,\mathrm{MWm}^{-1}$ in Jarrah (*Eucalyptus marginata*) forest is considered for the simulation. The fire behavior of the wildfire is summarized in Table 1.

Table 1. Summary of eucalyptus fire behavior for the experiment.

Avg. Intensity (I_{crown}) (kW/m)	Avg. RoS (m/s)	Avg Residence time(t_r) (s)	Canopy height (m)	Max. Flaming temp.(^{0}C)	Flame hght(m)
16 049	1.16	30	12	1200	20.8

A slight ambient wind of about $0.5\,\mathrm{m/s}$ at $10\,\mathrm{m}$ height was assumed so that flame tilt is negligible.This is an idealistic situation as crown fires of this intensity often occur in moderate to high wind velocities. Physical dimension of the simulated crown fire are shown in Fig. 5.
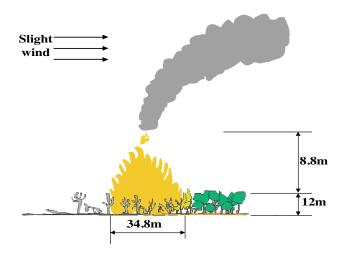
Figure 5. Physical dimensions of the wildfire used in the ray tracing simulation.

6.1.2. Flame Temperature and Ionization

The ray tracing considers only the continuous flame region of the plume, thus between 12 and 20 m above ground. Temperature decreases exponentially from a maximum of 1416 K at the canopy to 894 K at 20 m above ground level (Fig. 6).

With an average potassium content of 0.5% in vegetation, centerline electron density decreases from a maximum of the $3.40 \times 1016\,\mathrm{m}^{-3}$ within the eucalyptus canopy to $4.34 \times 1011\,\mathrm{m}^{-3}$ at 20 m above ground (Fig. 7). The ionization is influenced by temperature and the amount of potassium in the vegetation.

6.2. Simulated Radio Propagation in a Wildfire

A collimated radio wave (HF-VHF) beam was simulated to propagate through a very high intensity eucalyptus wildfire of physical dimension given in Fig. 5. The targeted area (receiver position) was 48.25 m from the transmitter. The scheme traced radio rays in small segments of 12.5 cm through the high intensity flame medium whose refractive index is spatially nonhomogeneous. Under normal conditions when there is no propagation path interception, the number of radio rays reaching the targeted area will be same as those leaving the transmitter. Temperature gradients in a wildfire environment deflect radio rays from the original path. The deflections consequently results in de-focusing or focusing of signal intensity at the targeted area.
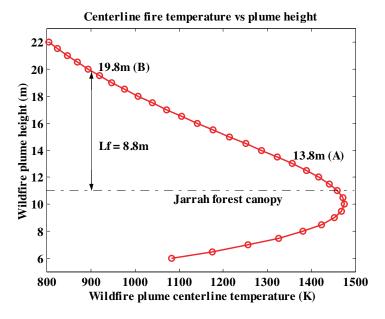
Centerline fire temperature vs plume height

Figure 6. Centerline temperature variation with plume height is the region up to 22 m.
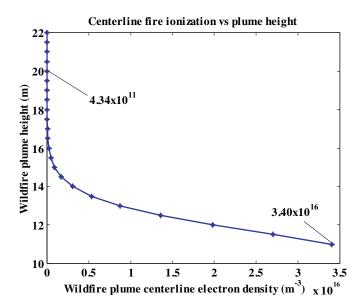
Centerline fire ionization vs plume height

Figure 7. Centerline plume ionization variation with plume.

As equi-spaced rays are representative of amplitude at the source, then the number radio rays reaching the target area (N_r) is directly proportion to signal amplitude (E_r) at the area, thus:

$$E_r = \zeta N_r \tag{23}$$

If N_t is the total number of rays targeted at the area (also proportional to intensity E_t), then attention due to deflection is given by:

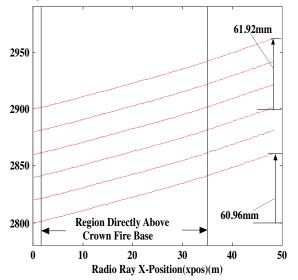$$\text{dB} = 20 \log \left(\frac{N_t}{N_r} \right) \tag{24}$$

The number of rays falling on the targeted area (N_r) is obtained by running the 2-D ray tracer model with rays spaced by a millimeter, shot at the same level as the target area. Rays falling on the area are identified and counted.

7. NUMERICAL RESULTS AND DISCUSSIONS
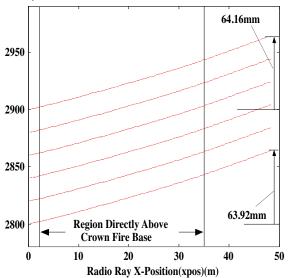
7.1. Ray Deflection in the Wildfire Environment

When a 150 MHz collimated beam of diameter 10 cm propagates at 0.8 m above the canopy of combusting vegetation with average potassium content of 0.5% (as in Australian sclerophyll forest), ray tracing scheme predicts top ray (tr) deflection of 48.56 mm from the targeted point 48 m from the transmitter. The scheme predicts a bottom ray (br) deflection of 44.66 mm from the targeted point. The procedure also predicts tr–br deflections of 61.92–60.96, 63.62–63.20, 63.88–63.54 and 64.16–63.92 mm for 450 (Fig. 8), 900, 1200 and 3000 MHz (Fig. 9) collimated beams respectively. According to the scheme, the 3000 MHz beam is the most refracted while the 150 MHz is the least deflected.

At 19.80, the ray tracing scheme predicts a tr–br deflection of 31.39–32.19 mm respectively for all frequencies in the range of 150–3000 MHz (e.g., in Fig. 10). A tr–br deflection of 17.98–17.94 mm respectively is predicted for all frequencies (150–3000 MHz) at 22.8 m above ground. A deflections of 17.98 (tr) and 17.94 (br) are predicted by the ray tracing scheme for 150–3000 MHz frequency range at the height of 22.8 m above ground (e.g., in Fig. 11). Deflections of 14.45 (tr) and 14.52 (br) are also predicted by scheme for 150–3000 MHz frequency range at the height of 32.8 m above ground (e.g., in Fig. 12). At 52.80 m above ground, the procedure predicts a tr deflection of 9.01 mm and a br deflection of 9.07 mm for all the frequency range (e.g., in Fig. 13). The simulation predicts tr is greater than br in the

Ray Trace of a Radio Wave Beam at 12.8m above Ground Level.

Figure 8. 450 MHz ray trace at 12.8 m above ground level.

Ray Trace of a Radio Wave Beam at 12.8m above Ground Level.

Figure 9. 3000 MHz ray trace at 12.8 m above ground level.

region up to 22.80 m above ground level. This is due to the influence of ionization on flame refractive index.

Ray deflections are observed to be generally highest in the hottest part of the plume and consequently reduce the signal amplitude at the targeted area. Signal loss due to refraction at the hottest part of the flame was observed to be frequency dependent (see Fig. 14).
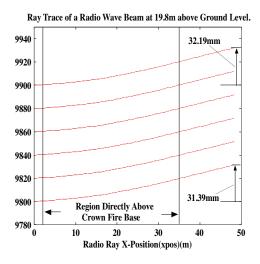

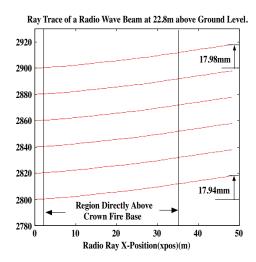**Figure 10.** 150 MHz ray trace at 19.8 m above ground level.
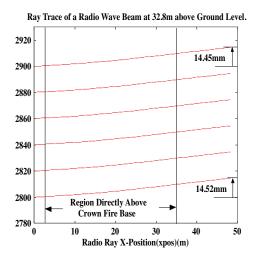

Figure 11. 1200 MHz ray trace at 22.8 m above ground level.

Ray Trace of a Radio Wave Beam at 32.8m above Ground Level.

14.45mm

Region Directly Above
Crown Fire Base

14.52mm

Radio Ray X-Position(xpos)(m)

Figure 12. 900 MHz ray trace at 32.8 m above ground level.

Ray Trace of a Radio Wave Beam at 52.8m above Ground Level.

9.01mm

Region Directly Above
Crown Fire Base
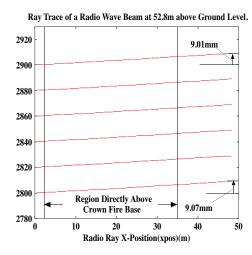
9.07mm

Radio Ray X-Position(xpos)(m)

Figure 13. 3000 MHz ray trace at 52.8 m above ground level.

Attenuation was observed to generally decrease with height above ground. At 19.8 m attenuation maintained a constant value of 3.4 dB even if the potassium content is increased up to 2.0%. For 22.8, 32.8 and 52.8 m above ground, attenuation was determined to maintained values of 1.66 dB and 0.92 dB respectively.
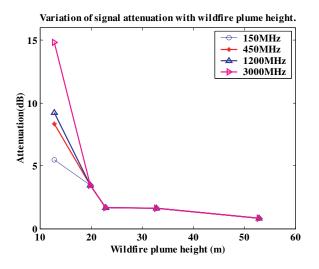
Variation of signal attenuation with wildfire plume height.

Figure 14. Signal attenuation due to refraction in a wildfire plume.

8. CONCLUSIONS

Radio waves that propagate in a plume of an intense wildfire were significantly affected by temperature or refractive index gradients. Deflections which ranged between 9.01 and 64.16 mm over a distance of 48.25 m were predicted by the 2D ray tracing scheme when rays propagate through a $90\,\mathrm{MWm}^{-1}$ wildfire plume. The deflection is frequency dependent at the hottest part (region up to 19.8 m above ground) of the plume where the influence of ionization is significant. The most affected was the 3000 MHz with maximum deflection of 64.16 mm at 12.8 m and the least affected was 150 MHz with a maximum deflection of 48.56 mm at the same height. The deflection caused a maximum signal strength loss between 5.47 dB and 14.84 dB for frequencies between 150 and 3000 MHz respectively at 12.8 m above ground. The signal strength losses were 3.45, 1.71, 1.64 and 0.85 dB for all frequencies (150–3000 MHz) at heights 19.8, 22.8, 32.8 and 52.8 m above ground respectively.

The frequency dependent deflections at the fire-fuel interface can seriously affect LOS ultra high frequency radio wave communications in wildfire environments. The observed deflections, e.g., 64.16 mm over 48.25 m for 3 GHz radio signals which cause signal loss of 14.84 dB, may not affect radio communication very much as 20 dB loss is tolerable. The fact that ray deflections vary exponentially with distance from the transmitter is a cause of great concern. Its implication is that

deflections and consequently attenuations could be large for LOS propagation of ultra high frequency radio waves at the interface. Attenuation in excess of $50\,\text{dB}$, which is highly probable from the predictions for propagation at the interface can seriously hamper radio communication for sets with omni directional antennas which are incapacitated to effectively receive from one direction.

The amount of ionization in the plume ranged from $3.40 \times 1016\,\text{m}^{-3}$ at the vegetation canopy-flame interface to $4.34 \times 1011\,\text{m}^{-3}$ at $20\,\text{m}$ above ground. This was enough to affect ray propagation path at least at below 19.8 above ground level.

ACKNOWLEDGMENT

REFERENCES

1. Akhtar, K., E. J. Scharer, S. M. Tysk, and E. Kho, "Plasma interferometry at high pressures," *Review of Scientic Instruments*, Vol. 74, No. 2, 996–1001, 2003.

2. Bean, B. R. and J. E. Dutton, "Radio meteorology," *Monogr.*, Vol. 92, 435, 1966.

3. Frost, L. S., "Conductivity of seeded atmospheric pressure plasmas," *Journal of Applied Physics*, Vol. 32, No. 10, 2029–2036, 1961.

4. Latham, D., "Space charge generated by wind tunnel fires," *Atmospheric Research*, Vol. 51, 267–278, 1999.

5. Ling, H., H. Kim, G. A. Hallock, B. W. Birkner, and A. J. M. Zaman, "Effect of an arc plume on satellite reflector performance," *IEEE Trans. Ant. and Prop.*, Vol. 39, No. 9, 1412–419, 1991.

6. Radojevic, M., "Chemistry of forest fires and regional haze with emphasis on southeast Asia," *Pure and Applied Geophysics*, No. 12, 157–187, 2003.

7. Raison, R. J., P. K. Khaina, and P. Woods, "Mechanisms of element transfer to the atmosphere during vegetation burning," *Canad. Journal of Forest Res.*, Vol. 15, 132–140, 1985.

8. Richerzhagen, B., "Finite element ray tracing: a new method

for raytracing in gradient index media," *Applied Optics*, Vol. 35, No. 3, 6186–6188, 1996.

9. Shuler, K. E. and J. Weber, "A microwave investigation of the ionization of hydrogen-oxygen and acetylene-oxygen flames," *Journal of Chemical Physics*, Vol. 22, No. 3, 491–502, 1954.

10. Sorokin, A., X. Vancassel, and P. Mirabel, "Emission of ions and charged soot particle by aircraft engines," *Atmos Chem. Phys. Dis.*, Vol. 2, 2045–2074, 2002.

11. Streifer, W. and K. B. Paxton, "Analytical solution of ray equation in cylindrical; inhomogeneous guiding media. 1. Meridonial rays," *Applied Optics*, Vol. 10, 769–775, 1971.

12. Weber, R. O., A. M. Gill, P. R. A. Lyons, and G. N. Mercer, "Time dependence of temperature above wildland fires," *CALM Science*, Vol. 4, 17–22, 1995.

13. Westberg, H. M., M. Bystrom, and B. Lecker, "Distribution of potassium, chlorine and sulphur between solid and vapour phases during combustion of wood and coal," *Energy and Fuels*, Vol. 17, 18–28, 2003.

14. Viegas, D. X., "Forest of propagation," *Phil. Trans. R. Soc. Lond. A.*, Vol. 356, 2907–2928, 1998.

15. Vodacek, A., R. L. Kremens, S. C. Fordham, S. C. VanGorden, D. Luisi, J. R. Schott, and D. J. Latham, "Remote optical detection of biomass burning using potassium emission signature," *Int. Journal of Remote Sensing*, Vol. 23, 2721–2726, 2002.

16. Williams, D. W., J. S. Adams, J. J. Batten, G. F. Whitty, and G. T. Richardson, "Operation Euroka: An Australian mass fire experiment," Report 386, Defense Standards Laboratory, Maribyrnor, Victoria Australia, 1970.

17. Foster, T., "Bushfire: history, prevention and control," A. H. and A. W. Reed, Pty. Ltd., 1976.

18. Hubner, G. and A. R. Jones, "Refractive index of flames in far infrared," *Journal of Phys. D: Appl. Phys.*, Vol. 6, 774–780, 1973.

19. Marchand, E. W., "Ray tracing in cylindrical gradient-index media," *Applied Optics Physics*, Vol. 11, 1104–1106, 1972.